PCCP

Accepted Manuscript

This is an *Accepted Manuscript*, which has been through the Royal Society of Chemistry peer review process and has been accepted for publication.

Accepted Manuscripts are published online shortly after acceptance, before technical editing, formatting and proof reading. Using this free service, authors can make their results available to the community, in citable form, before we publish the edited article. We will replace this *Accepted Manuscript* with the edited and formatted *Advance Article* as soon as it is available.

You can find more information about *Accepted Manuscripts* in the Information for Authors.

Please note that technical editing may introduce minor changes to the text and/or graphics, which may alter content. The journal's standard Terms & Conditions and the Ethical guidelines still apply. In no event shall the Royal Society of Chemistry be held responsible for any errors or omissions in this *Accepted Manuscript* or any consequences arising from the use of any information it contains.

ROYAL SOCIETY OF CHEMISTRY

www.rsc.org/pccp

Journal Name

ARTICLE TYPE

Cite this: DOI: 10.1039/xxxxxxxxxx

Efficient Electron-promoted Desorption of Benzene from Water Ice Surfaces†

Demian Marchione,*[a] John D. Thrower,[b] and Martin R. S. McCoustra[a]

Received Date
Accepted Date

DOI: 10.1039/xxxxxxxxxx

www.rsc.org/journalname

Desorption of benzene (C_6H_6) from solid water surfaces [compact amorphous solid water (c-ASW) and crystalline ice (CI)] during irradiation of ultrathin solid films with low energy (250-300 eV) electrons has been investigated. The observed desorption behaviour is complex but typically two desorption components, with particularly large cross-sections, were present in the observed signal. A fast component, with a cross-section up to 10^{-15} cm^2, is attributed to desorption of isolated C_6H_6 molecules that are hydrogen-bonded to small clusters of water (H_2O) molecules on the solid water surface. A slower component, with a cross-section of *ca.* 10^{-17} cm^2, is attributed mainly to desorption from larger C_6H_6 islands on the solid water surface. Possible desorption mechanisms are proposed and astrophysical implications are discussed.

1 Introduction

The impact of ionising radiation (keV and above charged particles and electromagnetic radiation with wavelengths shorter than 120 nm) on condensed phase aqueous environments is of both considerable practical and fundamental interest. The key role played in the chemical evolution of the Universe by cosmic ray interactions with icy dust grains and the radiological effects of ionising radiation on biological systems are but two examples. Primarily, ionising radiation interacts with condensed phase water by generating a cascade of low energy secondary electrons, which provide the crucial energy input for promoting physical and chemical change.[1,2] Though much is known of the mechanisms by which these electrons are generated in the condensed phase,[3] there remain gaps in our knowledge specifically surrounding the role low energy electrons play in promoting physico-chemical change especially in the interfacial or *selvedge* regions of the aqueous environment.[1,2]

Therefore, considerable effort has been devoted to investigating the processes underlying the low energy electron-promoted desorption (EPD) of neutral and ionic species from adsorbed layers of H_2O in recent years. A low threshold of *ca.* 5 eV, was found for the desorption of anionic H^- species from amorphous solid water (ASW) *via* the dissociative electron attachment (DEA) mechanism.[4] Frenkel-type excitons were implicated in desorption of H_2 at electron energies below 11 eV,[5] while the recombination of cationic species formed in the ice with quasi-free or trapped electrons was found to drive H_2 desorption at higher electron energies. Investigations of electron irradiation of thin ASW films deposited on Pt(111)[6,7] showed that H_2 formation is but one of the possible outcomes: O_2 production and desorption of intact H_2O molecules have also been observed. Frenkel-type excitons of $4a_1$ character lying near the bottom of the ice conduction band are thought to play an important role in the EPD of atomic fragments such as H (^{2}S), O (^{3}P$_2$) and O (^{1}D$_2$) from ASW films.[8] Formation of H_2, O_2 and H_2O_2 has also been reported at higher energies (5 keV) although these species remain trapped within the ice selvedge, and hence, are not observed during the irradiation but detected during subsequent thermal desorption.[9] More recent work has illustrated the desorption, promoted by low energy electrons, of simple species adsorbed on,[10] and absorbed in,[11] water ice.

Benzene (C_6H_6) is efficiently produced by ion chemistry in the upper atmosphere of Titan,[12,13] and it has been detected in the protoplanetary nebula CRL-618.[14] It is thought to form in the interstellar medium (ISM) under single collision conditions via the gas phase reaction of ethynyl radicals with 1,3-butadiene.[15] C_6H_6 is also proposed to be the starting point for the generation of polycyclic aromatic hydrocarbons (PAHs)[16,17] which carry a significant proportion of the interstellar carbon budget, although the efficiency of such synthetic process is still debated.[18,19] C_6H_6 itself is a convenient system for investigating the interaction of the π-electron density with H_2O ices. For instance, Zwier and co-workers[20–22] have presented IR data using resonance enhanced ionization techniques and resonant ion-dip IR spec-

*[a] *Institute of Chemical Sciences, Heriot-Watt University, EH14 4AS, Edinburgh, UK; E-mail: dm290@hw.ac.uk or marchionedemian@gmail.com*

[b] *Westfälische Wilhelms-Universität Münster, Münster, Germany; E-mail: john.thrower@uni-muenster.de*

[a] *Institute of Chemical Sciences, Heriot-Watt University, EH14 4AS, Edinburgh, UK; E-mail: m.r.s.mccoustra@hw.ac.uk*

† Electronic Supplementary Information (ESI) available: [details of any supplementary information available should be included here]. See DOI: 10.1039/b000000x/

Physical Chemistry Chemical Physics Accepted Manuscript

troscopy[23] to probe the intermolecular binding between C_6H_6 and $(H_2O)_n$ clusters. Theoretical investigations on the same systems by Slipchenko *et al.*[24] have highlighted that C_6H_6 behaves as both a donor and an acceptor of a hydrogen bond with H_2O. The interaction between C_6H_6 molecules and an H_2O ice film have also been considered. Previous temperature programmed desorption (TPD) studies of C_6H_6 on ASW show island formation during film growth from the lowest exposures.[25] This means that C_6H_6-C_6H_6 interaction is favoured over that between C_6H_6 and the ASW. Nonetheless, when the surface coverage is extremely low, deviation of the desorption kinetics from an ideal zero-order desorption, with evidence of a narrow range of desorption energies, at around 41.0 ± 0.5 kJ mol^{-1}, is compatible with the aromatic ring being π-hydrogen bonded in the sub-monolayer regime at the ice interface. Although not yet confirmed by theoretical studies,[26] reflection-absorption infrared (RAIR) spectra for similar coverages support this interpretation with some evidence of small shifts in peak position of the aromatic C-C stretch from that of bulk C_6H_6.[†,27]

In a previous letter, we reported our initial studies on the effect of low energy electrons on adlayers of C_6H_6 on ultrathin ASW films on amorphous silica.[10] We demonstrated that a highly efficient channel exists for the desorption of isolated C_6H_6 molecules from the ASW surface and a somewhat less efficient channel attributed to the desorption of C_6H_6 from C_6H_6 islands on the ASW surface. The cross-sections for both the processes were largely independent of incident electron energy in the range explored experimentally (100 eV - 350 eV); the observed small increase with primary electron energy is consistent with an increasing number of secondary electrons generated in the ASW film. In this paper, we more fully develop these studies to report on the effect of ASW film thickness and morphology in addition to the C_6H_6 coverage dependence. We discuss possible mechanisms for the observed C_6H_6 desorption and suggest that exciton-driven energy transfer from the bulk compact ASW to the selvedge plays an important role.

2 Experimental

The experiments described here were conducted in a stainless steel ultrahigh vacuum (UHV) chamber that has been described in detail elsewhere,[28,29] with a base pressure of approximately 2×10^{-10} Torr. The substrate is a polished stainless steel disk front-coated with *ca.* 200 nm of amorphous silica (SiO_2) that mimics the core of siliceous interstellar dust grains.[28] The disk was cooled by liquid nitrogen in a reservoir in thermal contact with the sample mount that gives a base temperature of 112 ± 2 K. Under these conditions, both exposure to an effusive molecular beam and background dosing results in growth of a compact, *i.e.* non-porous, ASW (c-ASW) film.[30,31] Deposition at 153 K results in a crystalline ice (CI) growth though a longer exposure (140 L) was necessary due to a non-negligible H_2O thermal desorption rate. In addition, H_2O was also deposited at base temperature and subsequently annealed to 138 K resulting in a film that has partially undergone the glass transition and it will be referred to as polycrystalline ice (PCI).[32–35] C_6H_6 vapour was subsequently deposited on top of the H_2O ice, with the sample at base temperature in all cases. Film thickness (d) is reported in Langmuir units ($1L = 1 \times 10^{-6}$ Torr s) and can be converted to

$$d = \frac{SPt}{\sqrt{2\pi m k_B T}} \frac{1}{\rho_s} \quad (1)$$

where S is the sticking coefficient assumed to be 1, k_B is the Boltzmann constant, T is the temperature of the dosed molecules, ρ_s is the molecular volume density, m is the mass, P is the pressure recorded on the hot cathode ion gauge corrected for the appropriate molecular ionisation efficiencies,[36] and t is the time of exposure. In the expression, we first define the number of molecules deposited onto the substrate (molecules per unit of surface area) during the dose and then divide this by the density (molecules per unit of volume). De-ionised H_2O and spectroscopic grade C_6H_6 (Fluka, ≥ 99.5%) were stored in glass vials and purified by repeated freeze-pump-thaw cycles before use.

Sample irradiation was performed using an electron gun (Kimball Physics, ELG-2) incident at 60° with respect to the substrate normal and over an area of 1 mm^2. Desorption of the species was followed using a quadrupole mass spectrometer (VG Microtech PC300D, further modified by ESS) with a homemade line-of-sight tube facing the front of the sample. Several control experiments revealed evidence of substrate charging during the irradiation of the ices with electrons. The incident electron current decreased by up to 30% after 600 s of exposure to the beam giving a typical average flux of $(9 \pm 2) \times 10^{13}$ electron cm^{-2} s^{-1}. However this had little impact on the quality of the reported measurements as the relevant events occur either in the first 50 s, when the flux can be assumed to be constant at around $(1.1 \pm 0.2) \times 10^{14}$ electron cm^{-2} s^{-1} (ϕ_1), or at longer times, when the flux has reached a limiting value of $(7.5 \pm 0.5) \times 10^{13}$ electron cm^{-2} s^{-1} (ϕ_2). No significant difference was noted between flux measurements made on the SiO_2 coated and the uncoated side of the substrate.

Monte Carlo simulations were performed to determine the electron penetration depth in pure C_6H_6 and ASW films using version 2.48 of the CASINO code.[37,38] Calculations for an incident beam at 60°, over an area of 1 mm^2, consistent with the experimental conditions (*e.g.* electron energy), showed that all the binary layered systems investigated have an overall larger thickness than the calculated electron maximum penetration depth. For example, assuming that the densities of the target molecular solids are 2.91×10^{22} molecule cm^{-3} and 8.57×10^{21} molecule cm^{-3} for H_2O and C_6H_6 respectively,[30,39] it is found that, for an energy of 250 eV, most of the incident electrons (∼ 85%) are stopped within the uppermost 5 nm of the ices. Distributions of electrons within the film as a function of the ASW depth for each experimental energy are reported in the ESI†.

3 Results and Discussion

3.1 Effect of Benzene Coverage

In order to investigate the mechanisms underlying the EPD of C_6H_6 from an underlying ASW film, we have re-investigated the dependence of the desorption signal on the thickness of the C_6H_6 overlayer. Previously we reported that desorption signal is dominated by a prompt rise immediately following the onset of electron irradiation.[10] This is shown in **Figure 1**, where for a small

Physical Chemistry Chemical Physics Accepted Manuscript

exposure of 0.5 L C_6H_6 on a thick ASW film the desorption signal clearly displays a single component that decays rapidly within the first 50 s of irradiation. We will subsequently refer to this as the fast desorption component. For small exposures, the resulting C_6H_6 film is expected to consist largely of isolated molecules and small islands interacting directly with the ASW surface. We have previously investigated the adsorption of C_6H_6 on ASW films using temperature programmed desorption.[25] As the exposure is increased island growth commences prior to the formation of 3-dimensional C_6H_6 structures and ultimately multilayer growth. This non layer-by-layer growth mechanism, along with the inherent roughness of the underlying ASW film results in the co-existence of C_6H_6 molecules adsorbed in these different growth phases at relatively large C_6H_6 exposure. Accordingly, as shown in **Figure 1**, the initial fast desorption component is still visible for a C_6H_6 exposure of 5 L along with an additional increase at longer times representing a much slower desorption process. As the film thickness is further increased to 50 L and beyond this component comes to dominate the desorption signal as the surface concentration of isolated C_6H_6 is reduced. With an exposure of 200 L the fast desorption peak is no longer present, consistent with the formation of a thick C_6H_6 film that completely covers the ASW substrate. The significantly reduced intensity of this desorption signal and much smaller desorption cross-section is consistent with the dominant electron-induced process in the C_6H_6 film being dehydrogenation and the formation of a graphitic deposit.[10] Previously we showed the desorption cross-section for the fast component to be of the order of 10^{-15} cm^2 and that this large cross-section can be related to the transfer of excitations within the ASW film to the interface region where C_6H_6 desorption from surface bound C_6H_6-$(H_2O)_n$ cluster is induced.

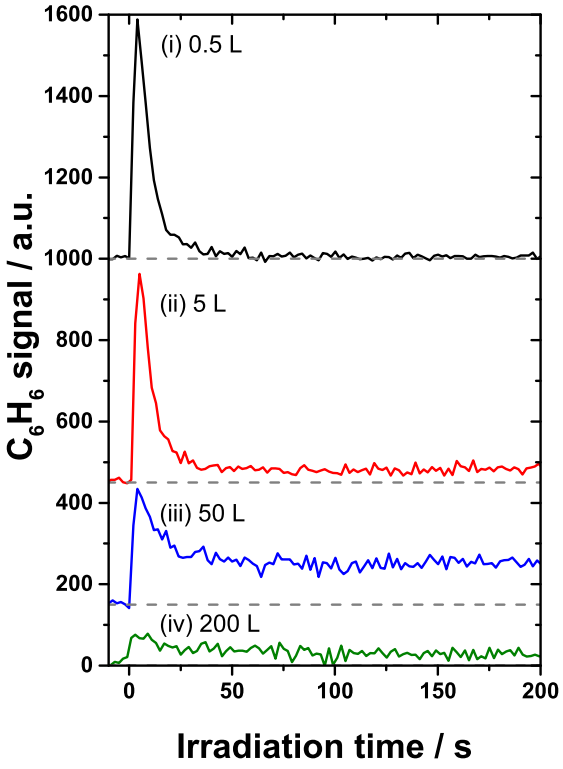

Fig. 1 C_6H_6 EPD traces for (i) 0.5, (ii) 5, (iii) 50 and (iv) 200 L of C_6H_6 adsorbed on a thick c-ASW film. The ices were irradiated with 300 eV electrons with a beam current of 100 nA. Traces are offset for clarity with the dashed lines showing the zero lines for each. The desorption signal for 200 L is clearly significantly reduced compared to the low coverage experiments. This highlights the role played by the c-ASW film in the desorption of C_6H_6 molecules.

3.2 Effect of Water Ice Film Thickness and Morphology

Since the efficient EPD of C_6H_6 requires the interaction of electrons with the underlying ASW underlayer, it follows that the role of the H_2O has to be carefully investigated. In principle, neglecting the direct interaction with the C_6H_6 molecules, the impinging electrons can promote excitations at the SiO_2/H_2O interface, within the bulk H_2O and/or at the H_2O/C_6H_6 interface. The excitation is subsequently transferred to the H_2O/C_6H_6 interface and ultimately the aromatic ring leading to non-thermal desorption. In order to elucidate some of the aspects of this process, a relatively thin film of C_6H_6 was deposited onto the H_2O ice films of varying thickness and phase (c-ASW, PCI, CI) and then irradiated with 250 eV electrons. Changing the H_2O thickness allows the investigation of the role of excitation within the bulk and at the SiO_2/H_2O interface while changing the phase probes the contribution made by dangling OH bonds at the H_2O/C_6H_6 interface in transferring the excitation itself.

3.2.1 ASW Film Thickness.

Irradiation experiments with 250 eV electrons were performed on layered binary ices comprising 5 L of C_6H_6 on ASW of variable thickness: 70 L (7.7 nm), 100 L (11 nm), 200 L (22 nm) and 500 L (55 nm). Given the results of the CASINO simulations (see the ESI†), $\sim$ 85% of the electrons at this energy are stopped within the top 5 nm of the ASW film. Thus, for ASW films thicker than 5 nm, no change should be expected in the EPD cross-sections as the bulk thickness of the ASW ice is increased and if the desorption process is specific to the H_2O/C_6H_6 interface.

Figure 2 shows the C_6H_6 desorption signal for the four ices. Consistently in all cases the intensity is highest as soon as the irradiation begins and quickly decays within the first 20 s. After that, a slow decrease culminates in a rather constant desorption rate that endures throughout the experiment. The irradiation was stopped before the signal reached zero. Since the beam spot (1 mm^2) is significantly smaller than the substrate itself (1 cm^2), diffusion from unirradiated areas occurs at 110 K, slowly repopulating with C_6H_6 the probed region of the sample. This explains the non-zero residual obtained in the fit. The observed trend, composed of fast and slow components, is consistent with the results presented in section 3.1.

In order to quantitatively estimate the EPD cross-section for C_6H_6 on ASW it is necessary to know both (i) the decay time constant, τ_i, which is given by the fit, and (ii) the current density, ϕ. The

Physical Chemistry Chemical Physics Accepted Manuscript

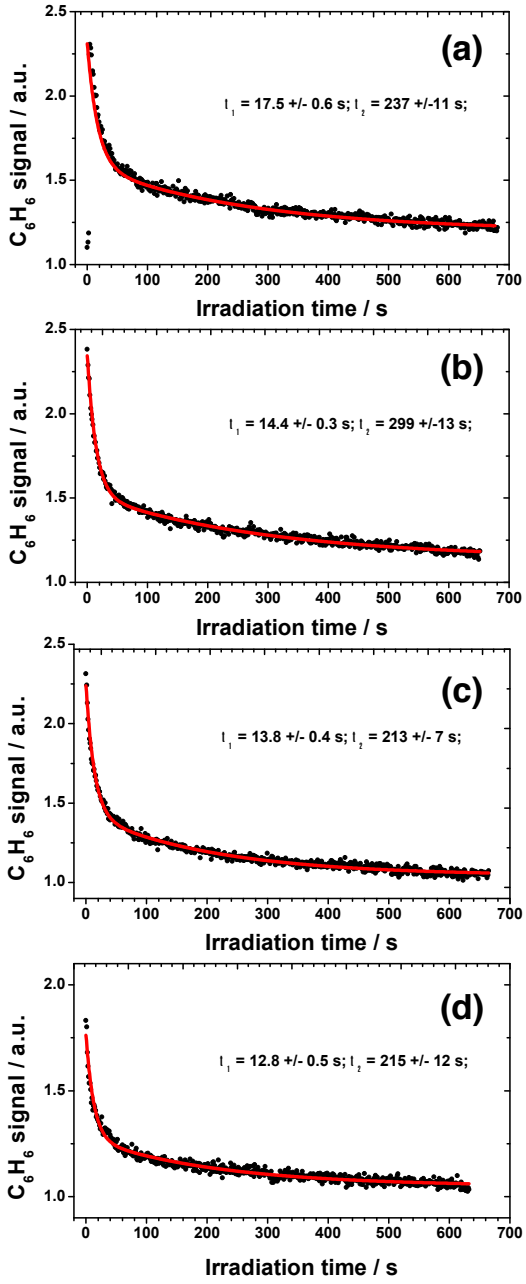

Fig. 2 C_6H_6 EPD signal obtained for 5 L of C_6H_6 on c-ASW of different thicknesses: a) 7.7 nm (70 L), b) 11 nm (100 L), c) 22 nm (200 L), and d) 55 nm (500 L). The experimental data are represented by black closed circles while the solid lines are the results of fitting a two component decay model to the data as described in the text. Irradiation was conducted with 250 eV electrons and initial beam current of 180 nA.

latter is the experimental electron flux in electron cm^{-2} s^{-1} and allow us to express τ_i in terms of desorption cross-section (σ_i) as it follows:

$$\sigma_i = \frac{1}{\tau_i \phi_i} \quad (2)$$

where the subscript i refers to the i^{th}-component in the multi-exponential decay describing the experimental data. In fact, by assuming first-order kinetics for the EPD process[40–42], we obtain σ_i and note that all the curves are well fitted by a bi-exponential decay function that explicitly contains two desorption components:

$$I(t) = I_1 e^{-\sigma_1 \phi_1 t} + I_2 e^{-\sigma_2 \phi_2 t} + I_\infty \quad (3)$$

where σ_i are the desorption cross-sections in cm^2 for the fast ($i = 1$) and slow ($i = 2$) component, I_i is the corresponding amplitude, while I_∞ is the residual. The values of the decay time constants, reported in **Figure 2**, are found to range from 13 to 18 seconds (mean of 14.5 ± 1.7 s) and from 213 to 299 seconds (mean of 241 ± 40 s) for the fast and slow process respectively. **Table 1** lists the electron fluxes employed in the measurements and the cross-sections obtained for this series of experiments. Note that due to the small amount of substrate charging observed, a lower current (120 ± 20 nA), and hence current density, was considered for the slow component. When both the statistical and experimental errors are taken into account, both σ_1 and σ_2 are independent of ASW film thickness for thicknesses greater than 70 L with mean values of $(6 \pm 2) \times 10^{-16}$ cm^2 and $(6 \pm 1) \times 10^{-17}$ cm^2 (see **Figure 3**). It can be concluded that the C_6H_6 non-thermal

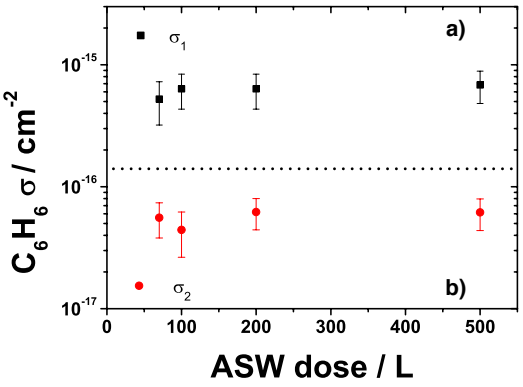

Fig. 3 Cross-section values and error bars of the fast (upper panel, a) and slow (lower panel, b) component in the EPD curve obtained for 5 L of C_6H_6 on c-ASW of different thicknesses: 7.7 nm (70 L), 11 nm (100 L), 22 nm (200 L), and 55 nm (500 L). Both σ_1 and σ_2 are reported in logarithmic scale: the former is represented in black squares, the latter in red closed circles. The dotted line is a guide to the eye as to enhance the difference in the order of magnitude between the two components.

desorption kinetics are independent of the thickness of the bulk H_2O films. This suggests that the energy which promotes desorption is deposited in the ASW film within 5 to 10 nm of the ASW/C_6H_6 ice and is transported to the interface initiating C_6H_6 desorption.

3.2.2 Effect of Water Ice Morphology.

Base temperature conditions in our apparatus (110 K) are compatible with the formation of a c-ASW layer. Annealing this later to 138 K allows the formation of an ice layer that is not yet fully crystalline and, hence, for the sake of clarity will be referred to as polycrystalline ice (PCI). Dosing at 153 K results in the growth of larger crystallites with a much reduced heterogeneity, and hence a CI film. However, at this temperature, the H_2O accommodation

Physical Chemistry Chemical Physics Accepted Manuscript

Table 1 Table listing values of electron fluxes, and cross-sections obtained from the experiments for the EPD process changing the c-ASW thickness.

Coverage/L	$\phi_1/10^{14}$ electron cm^{-2} s^{-1}	$\sigma_1/10^{-16}$ cm^2	$\phi_2/10^{13}$ electron cm^{-2} s^{-1}	$\sigma_2/10^{-17}$ cm^2
70	1.1 ± 0.2	5 ± 2	7.5 ± 0.7	5.6 ± 0.7
100	1.1 ± 0.2	6 ± 2	7.5 ± 0.7	4.4 ± 0.6
200	1.1 ± 0.2	6 ± 2	7.5 ± 0.7	6.2 ± 0.6
500	1.1 ± 0.2	7 ± 2	7.5 ± 0.7	6.2 ± 0.6

coefficient is reduced from 1. The loss was quantified to be *ca.* 36% by comparing the TPD areas for a fixed H_2O exposure at 110 K and 153 K. Therefore, in the latter case in order to compensate for the effect of desorption, a larger exposure (140 L) was used. As displayed in **Figure 4**, and in comparison to the other substrates, the CI substrate has a three-fold impact on desorption: (1) the fast initial event exhibits a modest rise in C_6H_6 intensity as irradiation begins; (2) from *ca.* 50 s up to 250 s, the C_6H_6 EPD signal is greater than on c-ASW; and (3) after *ca.* 350 s, the decay is faster than on the other substrates.

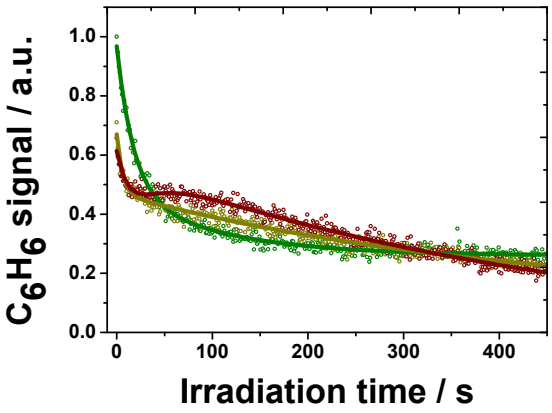

Fig. 4 C_6H_6 EPD signal obtained for 5 L of C_6H_6 on H_2O ice. H_2O condensed at 110 K results in a compact amorphous film (c-ASW, in green), annealing this to 138 K allows the formation of a film partially crystalline (PCI, in dark yellow), while higher deposition temperatures form a crystalline film (CI, in wine). Note that background dosing at 153 K leads to $\sim$ 36% loss of H_2O, therefore the substrate was exposed to H_2O vapour for longer, as to obtain a similar film thickness of the other experiments. Irradiation was conducted with 250 eV electrons and initial beam current of 180 nA. Fitted curves are displayed in full lines, while experimental points in open circles. A bi-exponential function was used for desorption traces from c-ASW and PCI, while a multi-exponential function best describes the remaining curve.

The observed trends appear to correlate with the degree of crystallinity within the H_2O ice layer. There is a progressive change in the desorption behaviour with increasing H_2O film growth temperature. Besides the decrease in the initial desorption intensity, the gradual appearance of a second increase between 50 and 100 s giving rise to a bump is noted: this is strongest for the CI, but is clearly absent for the c-ASW, while it appears to be present for the PCI substrate, where the rapid change in slope at *ca.* 25 s could be associated with the appearance of the delayed desorption component. Certainly, the remainder of the PCI curve is somewhat similar to that obtained for CI. Any differences observed in the EPD traces in the first instants of irradiation are likely to be linked to the impact that the phase has on the H_2O/C_6H_6 interface. At longer times, *ca.* 50 s onwards, the effects that the electron bombardment has on the ice structure itself should be taken into account. Previous studies have demonstrated that continuous exposure of CI to ionising sources (H^+, VUV, and especially electrons) leads to generation of an amorphous phase.[43–46] This might be reflected by the appearance of the bump in the EPD signal around 70 s as well as the faster decay after 350 s due to gradual electron induced changes to the ice morphology in the interface region.

In order to quantitatively evaluate the effect of the H_2O ice morphology on the C_6H_6 desorption, the EPD data were fitted with multi exponential functions. The bi-exponential expression in **Equation 3** was used for the curves resulting from deposition of H_2O as c-ASW (110 K) and PCI (138 K). However, this function is not sufficient to describe the more complex behaviour shown by the third curve in **Figure 4**. As in previous work,[10] the phenomenological equation that successfully replicates the appearance of a bump peaking around 70 s is:

$$I(t) = I_1 e^{-\sigma_1 \phi_1 t} + I_2 \left(e^{-\sigma_2 \phi_2 t} - e^{-\sigma_d \phi_2 t} \right) + I_\infty \qquad (4)$$

This expression is similar to **Equation 3**, but introduces a delay in the appearance of the second (slow) component with time decay constant τ_d from which we can derive a cross-section σ_d as per **Equation 2**. **Table 2** lists the values of cross-section found for the three curves distinguishing between the fast component (σ_1), the slow component (σ_2), and the delayed component (σ_d) when the latter clearly occurs. The σ_1 cross-sections for the experiments at 110 K and 153 K are consistent within the error bars. While σ_1 is larger, reaching a value of *ca.* 10^{-15} cm^2, for the PCI, this increase could be related to the presence of the underlying bump which is not intense enough to be revealed by the experimental curve, in such a way to allow the fit employing **Equation 4**, but might yet indirectly impact on the observed decay. In conclusion, there is no clear evidence for an increase in the cross-section for the fast component with the phase of the underlying ice. The slow component, σ_2, is almost halved going from c-ASW to CI; although overall this is a rather modest variation when the error bars are considered. It is important to stress that the C_6H_6 desorption from CI follows more complex

Table 2 List of cross-section values derived from the fits of the experimental EPD traces: C_6H_6 on CI, on PCI, and on c-ASW. In the latter case, the values are reported as average from the experiments in the previous section.

σ_T	$\sigma_1/10^{-16}$cm^2	$\sigma_2/10^{-17}$cm^2	$\sigma_d/10^{-16}$cm^2
$\bar{\sigma}_{110K}$	6 ± 2	6 ± 1	na
σ_{138K}	17 ± 4	3.2 ± 0.7	na
σ_{153K}	8 ± 2	2.9 ± 0.7	5 ± 1

Physical Chemistry Chemical Physics Accepted Manuscript

behaviour and having a delay cross-section σ_d comparable to σ_1. The appearance of this additional process leads to several effects on the EPD kinetics: (1) a further increase of the signal associated with this bump feature; (2) a delay in the appearance of the slow decay; and (3) determines a more effective depletion of C_6H_6 form the H_2O surface at shorter times (above 50 s), hence resulting in the trace to tending more quickly to zero at longer times ($>$ 400 s).

Clearly, CI has a much more ordered structure compared to the c-ASW. It is well-known from the literature that the coordination number of each hydrogen-bonded O-atom in the H_2O molecule is exclusively four in a perfect crystalline film, while amorphous phases display two-, three-, four- and even five-fold coordination.[47,48] This, combined with a less ordered structure, results in a larger number of H_2O/vacuum (hence H_2O/C_6H_6) interface dangling OH bonds for compact or porous ASW than for CI. It follows that a larger number of C_6H_6 molecules can be found directly bound to dangling bonds when the substrate is amorphous, and hence increasing the intensity of the rapid desorption signal. In conclusion, changing the phase of the H_2O ice underlying the C_6H_6 film strongly suggests that the mechanism is sensitive to the H_2O/C_6H_6 interface, although clearly there needs to be a sufficiently thick H_2O ice (bulk) film to accommodate the energy of the impinging electrons in the first instance before transferring that energy to the adsorbate. This could be confirmed by further EPD experiments using thinner ASW films which do not completely attenuate the electron beam. An identical interpretation to similar findings[49] has been proposed for the photodesorption (PD) of H_2O between 275 and 670 nm hinting to a common fundamental mechanism for non-thermal desorption at the H_2O surface.

3.3 Key Findings and Proposed Mechanism

The results presented in this and a previous[10] work on EPD of C_6H_6 from H_2O ices are summarised below, highlighting the key findings:

- EPD is dependent on the C_6H_6 coverage on the H_2O surface. At low exposures only one efficient process is observed ($\sigma_1 \simeq 10^{-15}$ cm^2), while this is quenched at large C_6H_6 exposures when the H_2O film is completely covered by a C_6H_6 multilayer. At intermediate coverages, desorption can be described using a multi-exponential decay that contains at least a fast and slow process.
- H_2O ice is a necessary substrate to observe the efficient desorption of the aromatic molecules.
- The process is independent of the thickness of the underlying H_2O ice in the range explored experimentally for thick films.
- The nature of the C_6H_6/H_2O interface is significant as it impacts on the intensity of the desorption trace and delays the slow desorption.

We now propose a qualitative model-mechanism to explain the large cross-section for non-thermal desorption of C_6H_6 from H_2O ices compatible with the key findings listed above. The starting point lies in the vast literature of previous studies on electron irradiation of icy films and on optical-absorption and electron-energy-loss spectroscopy (EELS) of solid and liquid water.[5,50–56]

The impinging electrons are energetic enough to pass through the entire C_6H_6 film and stop within the bulk of the H_2O film as demonstrated by simulations using the CASINO code (see ESI†). The primary energy loss mechanism is inelastic scattering leading to dipole excitation of the H_2O molecules and to their ionisation which produces a cascade of secondary electrons.[57,58] These will likely induce further multiple excitations, lying in the 8.7 eV - 21 eV range, and further ionisation events. In the work of Kimmel and Petrik,[5,6,58,59] molecular hydrogen (H_2) formation is observed following the irradiation of ASW with 100 eV electrons and was also observed during our measurements (results not shown). The formation and observation of H_2 is explained in terms of electronic excitation of the H_2O (exciton formation) and electronic energy transport to the H_2O/vacuum interface where H_2 formation occurs. Diffusion and long-range transport of H atoms through the ASW or dissociative electron attachment (DEA) reactions should not contribute significantly to the H_2 yield since the mobility of hydronium ions is very limited at 100 K[60] and because DEA would be efficient only at the H_2O/vacuum interface in a smaller energy range ($\sim$ 10 eV) than the 100 eV employed in the experiment.[61]

Based on this mechanism, the energy deposited in the ice in the form of long-lived excitons during irradiation, would be transported to the H_2O/C_6H_6 interface and promote non-thermal desorption of the aromatic molecules (see upper panel in **Figure 1**) competitively with H_2 formation. The energy is passed via π-hydrogen bond to the adsorbed aromatic molecule[25] promoting desorption (see the cartoon in **Figure 5**). It follows

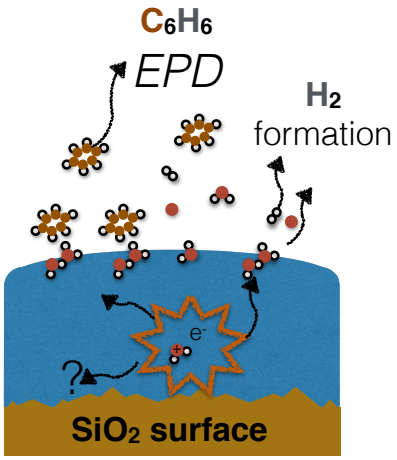

Fig. 5 Cartoon representing exciton formation in the solid H_2O bulk during electron irradiation and their migration to the vacuum interface leading to C_6H_6 desorption and H_2 formation. The question mark indicates unknown processes at the SiO_2/H_2O interface.

that the observed EPD is peculiar for adsorbates interacting with the H_2O surface *via* such a weak, directed interaction. Although further experiments are clearly necessary to confirm the role of

Physical Chemistry Chemical Physics Accepted Manuscript

the hydrogen bond at the interface and the hydrogen bonding network in the H_2O film. In contrast, as displayed in the lower panel in **Figure 1**, increasing the C_6H_6 coverages to form thick films (*e.g.* 200 L) reduces significantly the number of electrons reaching the underlaying H_2O. EPD promoted by interaction with H_2O is therefore quenched, while desorption of the adsorbates is still observed as it is activated by less efficient processes.[10] The value of σ_2, $(6 \pm 4) \times 10^{-17}$ cm^2, is consistent with previous studies of irradiation of both chemisorbed and multilayer C_6H_6 on W(110)[62] and of amorphous silica,[10] and hence, can be attributed to desorption from C_6H_6 multilayer on the solid H_2O surface. Although at intermediate exposures C_6H_6 forms islands, some molecules will still be H-bonded to the icy substrate leading to observation of both the fast and the slow desorption components. The latter does not simply contain the contribution to the signal from C_6H_6 desorbing from pure C_6H_6, but might be enhanced as a result of the islands disrupting, morphological changes within the ice, and non-thermal diffusion of islanded C_6H_6 towards the dangling OHs at the interface intensifying the desorption yield. Increasing the thickness of the H_2O film has no effect on the kinetics of the desorption, since if excitons were to form within the bulk and then migrate isotropically in all directions, those travelling toward the H_2O/C_6H_6 would not be affected by a larger spacing below 7 - 8 nm of depth. However, in **Figure 2** the curve for 500 L of c-ASW, the initial rise is less intense compared to thinner H_2O films (70 L, 100 L, and 200 L). This is interpreted as due to the available surface area at the interface; a thinner H_2O film would reflect peaks and troughs of the underlying substrate, while these would be smoothed out in thicker films. A smaller degree of surface roughness means a reduced surface area at the interface, and hence fewer sites where C_6H_6 molecules could be hydrogen-bonded and accept the energy deposited in the bulk during the irradiation.

The same interpretation can be extended to the bump appearing in **Figure 4** and in previous work.[10] In the latter case this feature was observed also for C_6H_6 on c-ASW when high electron energies were used (*e.g.* 350 eV). Irradiation dynamically changes (roughens) the H_2O surface and generates additional dangling bonds that coordinate to the aromatic rings. This leads to a further increase of the desorption rate in the form of the aforementioned bump. This process can be particularly efficient, with a cross-section of $\sim 10^{-16}$ cm^2, and depends on the phase of the H_2O ice and on the energy of the impinging electrons. The exact mechanism is not yet clear, however the data are consistent with the idea that the entity in which the icy surface roughens correlates with a more or less efficient rearrangement of the H_2O/vacuum interface. This is due to amorphisation of the H_2O/vacuum interface accompanied by disruption of the C_6H_6 islands when the electron energy is highest and the morphology changes most. Hence, it follows that diffusion of the aromatic molecules from the edges of the islands themselves to the newly generated dangling OHs promotes the second increase (bump) in the EPD traces.

4 Astrophysical Implications and Conclusions

The experiments discussed in this work simulate the secondary electron flux forming subsequent to ionising radiation interaction with interstellar ices. There are several sources that could lead to ionisation and, hence, to secondary electrons: X-rays, γ-rays, cosmic rays and to some extent also energetic VUV photons. Particularly noteworthy is the case of cosmic ray protons where the differential flux exhibits a relatively flat distribution between 1 - 100 MeV, with a maximum at 50 MeV.[63] The integrated flux is $\sim$ 1 cm^{-2} s^{-1} in this energy range. The distribution of secondary electrons produced by primary ions (^{1}H, ^{4}He) in liquid water is only slightly dependent on the energy of the ions themselves between 100 keV and 100 MeV.[57] These energy distribution curves, with a mean electron energy between 38.6 eV and 65.1 eV, overlap with the electronic excitations of solid H_2O at 8.7 eV, 10.4 eV and 14.5 eV, and 21 eV. Although these distributions were obtained from liquid water, they are not expected to be significantly different in ASW, which has often been used in the past as a model of liquid phase.[1] Therefore, it can be concluded that cosmic rays impacting the icy ISM grain mantles, mostly made of H_2O, produce an ionisation track within the mantle which is rich in secondary electrons having energies resonant with valence electronic excitations of solid H_2O. The primary electron beam used in the experiments reported herein would likely be inelastically scattered, ionising molecules and forming a similar flux of secondary electrons to that associated with cosmic rays; thought somewhat more localised in the selvedge that would be the case for cosmic ray irradiation. Therefore, the reported results are appropriate for consideration in an astrophysical context.

It should be stressed that the relative abundance of C_6H_6 in dense clouds is not sufficient for the formation of thick layers, however, solid H_2O is certainly the main component of the ice mantles and presents peculiarities (long-lived exciton formation) that could favour EPD of any small molecule, including carbon monoxide (CO) which is known to be weakly bound to the ice surface *via* a dangling OH bond.[64–66] The key point is that the efficiency of the desorption process observed in the present work results from the deposition of energy in the underlying H_2O film rather than the nature of the adsorbate film. Although dedicated measurements are clearly required, it is therefore reasonable to consider that a similar efficient desorption may occur for other adsorbates bound on a H_2O substrate. Therefore, the surface abundance of a molecule such as CO on the ASW would be the result of several processes: adsorption from the gas phase; thermal and non-thermal desorption; and reactions on the surface. It is noteworthy that hydrogenation of CO is the first and crucial step to the reactive accretion of complex organic molecule (COM) on the ISM grain surface. Clearly an additional efficient desorption step might potentially delay the mantle enrichment in CO, and hence methanol (CH_3OH) formation, and thence other organic molecules.

In order to ascertain the impact of EPD from ASW on an astrophysically relevant time-scale, it is desirable to quantitatively compare the effectiveness of EPD and photodesorption (PD) of

Physical Chemistry Chemical Physics Accepted Manuscript

just CO on ASW at sub-monolayer, and monolayer level. Fayolle *et al.*[67] have reported an average value of 1.8×10^{-2} molecule photon^{-1} for PD yields of CO from CO multilayers in the investigated range (120 - 177 nm). This process was shown to be independent of the thickness of the CO ice confirming that only the top few layers are directly involved. No direct measurements for the PD of CO from ASW are available as to date, thus we will assume that, in contrast with the EPD process, the H_2O substrate has no effect on the PD yield of the adsorbate (CO). In order to compare these findings with the EPD results, the CO PD rate, k_{PD}^{CO}, can be estimated under astrophysical conditions using the following equation:

$$k_{PD}^{CO} = \Phi \sigma_{abs} F_{VUV} \quad (5)$$

where Φ is the yield of the process (1.8×10^{-2}); σ_{abs} is the photon absorption cross-section for CO in the VUV range between 120 nm and 160 nm (4.7×10^{-18} cm^2);[68] and F_{VUV} is the estimated VUV flux in dense clouds. The latter, is dominated by the emission from H_2 excited by cosmic rays and is typically[63,69] about 5×10^3 photon cm^{-2} s^{-1}. Therefore a rate of 4.2×10^{-16} s^{-1} is obtained.

To estimate the EPD rate for CO from ASW is less straightforward and requires that a few assumptions to be made:

1. CO bonds weakly to the ASW surface *via* a hydrogen bond like interactions through dangling OH on the ASW surface. EPD occurs *via* the same mechanism for CO as for C_6H_6.

2. Only the fast desorption process will be considered as this relates to isolated molecules on the ASW surface and it might be more relevant to astrophysical irradiation time-scales.

3. The cross-section is assumed to be the same as for C_6H_6 (10^{-15} cm^2).

4. The flux of secondary electrons, F_{e^-}, produced by cosmic rays in 5 nm of c-ASW can be estimated using the SRIM code[70,71] for a flux of 1 cm^{-2} s^{-1} 1 MeV H^+ ions and this is 4.5 electron cm^{-2} s^{-1} (see ESI†).

5. The energy deposited per ionisation event is assumed to be twice the ionisation potential of the target molecule being ionised (11.0 eV).[72,73]

6. Few isolated CO molecules are adsorbed on the ASW surface. Thus, no direct effect of the incoming ions will be considered on CO, which will be assumed to be "transparent".

The EPD rate constant, k_{EPD}^{CO}, is defined as:

$$k_{EPD}^{CO} = \sigma F_{e^-} \quad (6)$$

and its value is 4.5×10^{-15} s^{-1}. The ratio between the two non-thermal desorption rates is

$$\frac{k_{EPD}^{CO}}{k_{PD}^{CO}} = 11 \quad (7)$$

The fast EPD process is thus about one order of magnitude more efficient than PD in dense clouds. Thus, the presence of this efficient desorption channel means that the EPD of an adsorbate, such as CO, on ASW cannot be ignored and should be taken into account in more complete astrochemical models as much as other non-thermal processes. Future works are in preparation to further expand on the astrophysical relevance of these results.

In conclusion, our results confirm the already reported high EPD cross-section of C_6H_6 from H_2O ices and provide additional support for the proposed mechanism involving exciton transport to the H_2O/vacuum interface. In addition we have discussed the possible astrophysical impact of our observations on CO accretion and subsequent hydrogenation on the icy ISM dust grains. CO depletion would be faster than currently believed which in turn will slow the formation of hydrogenated CO derivatives and, hence, slow the radiation-driven formation of COM.

5 Acknowledgements

The authors acknowledge the support of the UK Engineering and Physical Sciences Research Council (EPSRC) and the European Community FP7-ITN Marie-Curie Programme (LASSIE project, grant agreement #238258). Financial support from Heriot-Watt University for a number of upgrades to the UHV system is also acknowledged.

References

1 B. C. Garrett, D. A. Dixon, D. M. Camaioni, D. M. Chipman, M. A. Johnson, C. D. Jonah, G. A. Kimmel, J. H. Miller, T. N. Rescigno, P. J. Rossky, S. S. Xantheas, S. D. Colson, A. H. Laufer, D. Ray, P. F. Barbara, D. M. Bartels, K. H. Becker, K. H. Bowen, S. E. Bradforth, I. Carmichael, J. V. Coe, L. R. Corrales, J. P. Cowin, M. Dupuis, K. B. Eisenthal, J. A. Franz, M. S. Gutowski, K. D. Jordan, B. D. Kay, J. A. LaVerne, S. V. Lymar, T. E. Madey, C. W. McCurdy, D. Meisel, S. Mukamel, A. R. Nilsson, T. M. Orlando, N. G. Petrik, S. M. Pimblott, J. R. Rustad, G. K. Schenter, S. J. Singer, A. Tokmakoff, L.-S. Wang and T. S. Zwier, *Chem. Rev.*, 2005, **105**, 355–390.

2 E. Alizadeh and L. Sanche, *Chem. Rev.*, 2012, **112**, 5578–5602.

3 J. Savolainen, F. Uhlig, S. Ahmed, P. Hamm, and P. Jungwirth, *Nature*, 2014, **6**, 697–701.

4 P. Rowntree and L. Parenteau, L. Sanche, *J. Chem. Phys.*, 1991, **94**, 8570–8576.

5 G. A. Kimmel, T. M. Orlando, C. Vézina and L. Sanche, *J. Chem. Phys.*, 1994, **101**, 3282–3286.

6 N. G. Petrik and G. A. Kimmel, *J. Chem. Phys.*, 2005, **123**, 054702.

7 N. G. Petrik, A. G. Kavetsky and G. A. Kimmel, *J. Chem. Phys.*, 2006, **125**, 124702.

8 T. M. Orlando and G. A. Kimmel, *Surf. Sci.*, 1997, **390**, 79–85.

9 W. Zheng, D. Jewitt and R. I. Kaiser, *Astrophys. J.*, 2006, **639**, 534–548.

10 J. D. Thrower, M. P. Collings, F. J. M. Rutten and M. R. S. McCoustra, *Chem. Phys. Lett.*, 2011, **505**, 106–111.

11 N. G. Petrik, R. J. Monckton, S. P. K. Koehler and G. A. Kimmel, *J. Chem. Phys.*, 2014, **140**, 204710.

Physical Chemistry Chemical Physics Accepted Manuscript

12 V. Vuitton, R. V. Yelle and P. Lavvas, *Phil. Trans. R. Soc. A*, 2009, **367**, 729–741.

13 M. L. Delitsky and C. P. McKay, *Icarus*, 2010, **207**, 477–484.

14 J. Cernicharo, A. M. Heras, A. Tielens, J. R. Pardo, F. Herpin, M. Guélin and L. B. F. M. Waters, *Astrophys. J.*, 2001, **546**, L123–L126.

15 B. M. Jones, F. Zhang, R. I. Kaiser, A. Jamal, A. M. Mebel, M. A. Cordiner and S. B. Charnley, *Proc. Natl. Acad. Sci. U. S. A.*, 2010, **108**, 452–457.

16 H. Bockhorn, F. Fitting, H. W. Wenz and B. Bunsenges, *Ber. Bunsenges. Phys. Chem.*, 1984, **20**, 1067–1073.

17 M. Frenklach, D. W. Clary, W. C. Gardiner and S. E. Stein, *Proc. Combust. Inst.*, 1984, **20**, 887–901.

18 A. G. G. M. Tielens, *Rev. Mod. Phys.*, 2013, **85**, 1021–1081.

19 P. Merino, M. Švec, J. I. Martinez, P. Jelinek, P. Lacovig, M. Dalmiglio, S. Lizzit, P. Soukiassian, J. Cernicharo and J. A. Martin-Gago, *Nat. Commun.*, 2014, **5**, 1–9.

20 A. J. Gotch, A. W. Garrett, D. L. Severance and T. S. Zwier, *Chem. Phys. Lett.*, 1991, **178**, 121–129.

21 A. J. Gotch and T. S. Zwier, *J. Chem. Phys.*, 1992, **96**, 3388–3401.

22 A. J. Garrett and T. S. Zwier, *J. Chem. Phys.*, 1992, **96**, 3402–3410.

23 R. N. Pribble and T. S. Zwier, *Faraday Discuss.*, 1994, **97**, 229–241.

24 L. V. Slipchenko and M. S. Gordon, *J. Phys. Chem. A*, 2009, **113**, 2092.

25 J. D. Thrower, M. P. Collings, F. J. M. Rutten and M. R. S. McCoustra, *J. Chem. Phys.*, 2009, **131**, 244711.

26 D. Sharma and M. J. Paterson, *Photochem. Photobiol. Sci.*, 2014, **13**, 1549–1560.

27 J. D. Thrower, *PhD thesis*, Heriot-Watt University, 2009.

28 J. D. Thrower, M. P. Collings, F. J. M. Rutten and M. R. S. McCoustra, *Mon. Not. R. Astron. Soc.*, 2009, **394**, 1510–1518.

29 A. G. M. Abdulgalil, D. Marchione, J. D. Thrower, M. P. Collings, M. R. S. McCoustra, I. F., M. E. Palumbo, E. Congiu and F. Dulieu, *Phil. Trans. R. Soc. A*, 2013, **371**, 20110586.

30 G. A. Kimmel, Z. Dohnálek, K. P. Stevenson, R. S. Smith and B. D. Kay, *J. Chem. Phys.*, 2001, **114**, 5295–5303.

31 M. S. Westley, G. A. Baratta and R. A. Baragiola, *J. Chem. Phys.*, 1998, **108**, 3321–3326.

32 J. A. McMillan and S. C. Los, *Nature*, 1965, **206**, 806–807.

33 M. Sugisaki, H. Suga and S. Seki, *Bull. Chem. Soc. Jpn.*, 1968, **41**, 2591–2599.

34 P. Jenniskens, S. F. Banham, D. F. Blake and M. R. S. McCoustra, *J. Chem. Phys.*, 1997, **107**, 1232–1241.

35 A. Yabushita, D. Kanda, N. Kawanaka, M. Kawasaki and M. N. Ashfold, *J. Chem. Phys.*, 2006, **125**, 133406.

36 R. L. Summers, *Empirical observations on the sensitivity of hot cathode ionization type vacuum gauges*, National Aeronautics and Space Administration, Washington, D. C., 1969.

37 *Theory of Condensed Matter Group Cambridge, CASINO V 2.48*, http://www.gel.usherbrooke.ca/casino/What.html, 2014.

38 P. Hovington, D. Drouin and R. Gauvin, *Scanning*, 1997, **19**, 1–14.

39 C. J. Craven, P. D. Hatton, C. J. Howard and G. S. Pawley, *J. Chem. Phys.*, 1993, **98**, 8236–8243.

40 S. W. Bellard and E. M. Williams, *Surf. Sci.*, 1979, **80**, 450–458.

41 L. K. Verheij, J. Lux, A. B. Anton, B. Poelsema and G. Comsa, *Surf. Sci.*, 1987, **182**, 390–410.

42 K. Golibrzuch, P. R. Shirhatti, J. Geweke, J. Werdecker, A. Kandratsenka, D. J. Auerbach, A. M. Wodtke and C. Bartels, *J. Am. Chem. Soc.*, 2015, **137**, 1465–1475.

43 M. H. Moore, *Astrophys. J.*, 1992, **401**, 353–360.

44 G. Strazzulla, G. A. Baratta, G. Leto and G. Foti, *Europhys. Lett.*, 1992, **18**, 517–522.

45 G. Leto and G. A. Baratta, *Astron. Astrophys.*, 2003, **397**, 7–13.

46 W. Zheng, D. Jewitt and R. I. Kaiser, *J. Phys, Chem. A*, 2009, **113**, 11174–11181.

47 P. Jenniskens, D. F. Blake, M. A. Wilson and A. Pohorille, *Astrophys. J.*, 1995, **455**, 389–401.

48 J. A. Noble, C. Martin, H. J. Fraser, P. Roubin and S. Coussan, *J. Phys. Chem. C*, 2014, **118**, 20488–20495.

49 J. Bergeld and D. Chakarov, *J. Chem. Phys.*, 2006, **125**, 141103.

50 A. Otto, M. J. Lynch and J. Aust, *Phys.*, 1970, **23**, 609–612.

51 M. Heller, R. N. Hamm, R. D. Birkhoff and L. R. Painter, *J. Chem. Phys.*, 1974, **60**, 3483–3486.

52 J. Daniels, *Opt. Commun.*, 1971, **3**, 240–243.

53 J. A. LaVerne and A. Mozumder, *Radiat. Res.*, 1993, **133**, 282–288.

54 C. D. Wilson, C. A. Dukes and R. A. Baragiola, *Phys. Rev. B*, 2001, **63**, 121101.

55 R. D. Leapman and S. Sun, *Ultramicroscopy*, 1995, **59**, 71–79.

56 K. Kobayashi, *J. Phys. Chem.*, 1983, **87**, 4317–4321.

57 S. Pimblott and J. Verne, *Rad. Phys. and Chem.*, 2007, **423**, 1244–1247.

58 N. G. Petrik and G. A. Kimmel, *Phys. Rev. Lett.*, 2003, **90**, 166102.

59 N. G. Petrik and G. A. Kimmel, *J. Chem. Phys.*, 2004, **121**, 3727–3735.

60 J. P. Cowin, *Nature*, 1999, **398**, 405–407.

61 G. A. Kimmel and T. M. Orlando, *Phys. Rev. Lett.*, 1996, **77**, 3983–3986.

62 J. E. Whitten and R. Gomer, *Surf. Sci.*, 1996, **347**, 280–288.

63 C. J. Shen, J. M. Greenberg, W. A. Schutte and E. F. van Dishoeck, *Astron. Astrophys.*, 2004, **415**, 203–215.

64 M. P. Collings, J. W. Dever, H. J. Fraser, M. R. S. McCoustra and D. A. Williams, *Astrophys. J.*, 2003, **583**, 1058–1062.

65 H. J. Fraser, M. P. Collings, J. W. Dever and M. R. S. McCoustra, *Mon. Not. R. Astron. Soc.*, 2004, **353**, 59–682.

66 M. P. Collings, J. W. Dever and M. R. S. McCoustra, *Phys. Chem. Chem. Phys.*, 2014, **16**, 3479–3492.

67 E. C. Fayolle, M. Bertin, C. Romanzin, X. Michaut, K. I. Öberg,

Physical Chemistry Chemical Physics Accepted Manuscript

H. Linnartz and J.-H. Fillion, *Astrophys. J. Lett.*, 2011, **739**, L36.

68 G. A. Cruz-Diaz, G. M. M. Caro and T. S. Chen, Y. J.and Yih, *Astron. Astrophys.*, 2014, **562**, A119.

69 J. . Mathis, . G. Mezger and N. Panagia, *Astron. Astrophys.*, 1983, **128**, 212–229.

70 J. F. Zigler, *SRIM/TRIM*, http://www.srim.org, 2013.

71 J. F. Ziegler, J. P. Biersack and M. D. Ziegler, *The Stopping and Range of Ions in Solids*, Pergamon Press, New York, 2008.

72 W. F. Schmidt and E. Illenberger, *Nukleonika*, 2003, **48**, 75–82.

73 M. Vinodkumar, K. N. Joshipura, C. G. Limbachiya, and B. K. Antony, *Nucl. Instrum. Methods Phys. Res. B*, 2003, **212**, 63–66.

Physical Chemistry Chemical Physics Accepted Manuscript